Optical coherence tomography speckle decorrelation for detecting cell death

Golnaz Farhat[a,b], Adrian Mariampillai[d,e], Victor X. D. Yang[b,d], Gregory J. Czarnota[a,b,c] and Michael C. Kolios[a,f]
[a]Dept. of Medical Biophysics, University of Toronto, Toronto, Canada;
[b]Imaging Research and [c]Radiation Oncology, Sunnybrook Health Sciences Centre, Toronto, Canada;
[d]Dept. of Electrical & Computer Engineering, Ryerson University, Toronto, Canada;
[e]Ontario Cancer Institute, University Health Network, Toronto, Canada;
[f]Dept. of Physics, Ryerson University, Toronto, Canada;

ABSTRACT

We present a dynamic light scattering technique applied to optical coherence tomography (OCT) for detecting changes in intracellular motion caused by cellular reorganization during apoptosis. We have validated our method by measuring Brownian motion in microsphere suspensions and comparing the measured values to those derived based on particle diffusion calculated using the Einstein-Stokes equation. Autocorrelations of OCT signal intensities acquired from acute myeloid leukemia cells as a function of treatment time demonstrated a significant drop in the decorrelation time after 24 hours of cisplatin treatment. This corresponded with nuclear fragmentation and irregular cell shape observed in histological sections. A similar analysis conducted with multicellular tumor spheroids indicated a shorter decorrelation time in the spheroid core relative to its edges. The spheroid core corresponded to a region exhibiting signs of cell death in histological sections and increased backscatter intensity in OCT images.

Keywords: cell death, apoptosis, dynamic light scattering, optical coherence tomography, autocorrelation, decorrelation time, Brownian motion, tumor spheroid

1. INTRODUCTION

Speckle in optical coherence tomography (OCT) images results from light backscattered by multiple scatterers within a resolution volume (RV) of the imaging system [1]. Speckle intensity depends on the number, size, optical properties and spatial distribution of these scatterers. Imaging of living cells and tissues can produce changes in the speckle pattern due to the motion of subresolution scatterers [2, 3]. In addition to the presence of red blood cells flowing within the vasculature, scatterer motion in tissue can be caused by intracellular motion. Examples include the movement of organelles along microtubules necessary for processes involved in cell homeostasis, the reorganization of cellular contents in preparation for mitosis, the process of mitosis, and the morphological changes that occur during apoptosis.

Apoptosis is a process by which a predictable sequence of biochemical and morphological changes lead to cell death. It is essential in human development and homeostasis and many cancer therapies take advantage of this form of cell death in proliferating cancer cells to reduce tumor burden and cure patients. Morphologically, apoptosis is characterized by a rounding and shrinking of the cell, fragmentation of the nucleus and other organelles, membrane blebbing and, ultimately, disintegration of the cell into intact membrane-bound fragments called apoptotic bodies [4]. We hypothesize that the rate of intracellular motion in apoptotic cells will be higher than in viable cells due to the remodeling of the cytoskeleton required for membrane blebbing and cell fragmentation, and predict that this increase in intracellular motion can be detected using principles of dynamic light scattering (DLS) adapted to OCT.

Dynamic light scattering techniques are based on measuring the time-dependent fluctuations in scattered light intensity from a sample and relating these fluctuations to physical properties of that sample. This technique has been used to determine properties such as size distribution, molecular weights and rotational motion of particles in suspension or macromolecules in solution [5]. Dynamic laser-light scattering has been applied to the characterization of biological systems, measuring bacterial growth [6] and human sperm motility [7] through the measurement of velocity distributions

Biomedical Applications of Light Scattering V, edited by Adam P. Wax, Vadim Backman,
Proc. of SPIE Vol. 7907, 790710 · © 2011 SPIE · CCC code: 1605-7422/11/$18 · doi: 10.1117/12.874682

as well as to determine blood flow velocities [8]. Blood flow measurements using DLS have also been implemented in a pig model as a method to assess the depth of skin burns [9]. Coherence-domain digital holography has since been applied to the capture of intracellular motion in tumor spheroids [10].

The work described in this study demonstrates a technique to measure the rate of decorrelation of speckle in multiple consecutive OCT images obtained using a swept-source OCT system with a 1300 nm light source. Our laboratory has previously proposed using changes in the characteristics of OCT backscatter to characterize cellular viability, and has shown that significant changes in scattering strength occur during cell death [11]. Recent experiments using single cell acoustic microscopy (for which the ultrasonic wavelengths approach 1 μm) indicated rapid variations in cellular structure during apoptosis based on the ultrasonic speckle decorrelation [12]. We, therefore, hypothesize that a similar phenomenon can be observed using OCT, with the added advantage of higher data acquisition rates. Moreover, we expect to derive complementary information as a result of the difference in optical and ultrasonic contrast mechanisms.

Our speckle decorrelation method was validated by measuring the decorrelation time (DT) caused by Brownian motion in monodisperse microsphere suspensions and comparing these to theoretical values calculated from the Einstein-Stokes equation. In order to avoid complications in the interpretation of speckle decorrelation introduced by blood flow, we tested our method in biological models based on pure cell aggregates. In the first model acute myeloid leukemia (AML) cells were centrifuged to create a densely packed cell sample [13]. In the second model, multicellular tumor cell spheroids (MCTS) were generated from a human colorectal cancer cell line (HT-29). The tumor spheroid is an *in vitro* three dimensional cell culture system often used to model the *in vivo* growth properties of tumors. These cell aggregates are typically composed of a core of quiescent cells surrounded by an outer rim of proliferating cells. As the spheroid grows beyond 400-500 μm in diameter a central zone of cell death begins to form as a consequence of nutrient deprivation caused by the inability of oxygen and growth medium to penetrate to its core. This region becomes necrotic with continued spheroid growth [14]. It has been shown that cell death in the core of HT-29 MCTS is induced by apoptosis [15].

2. METHODS

2.1 OCT system

Optical coherence tomography images and data were acquired using a Thorlabs Inc. (Newton, NJ) swept source OCT (OCM1300SS) system. This system uses a frequency swept external cavity laser with a central wavelength of 1325 nm, a -3 dB bandwidth of approximately 100 nm and an average output power of 10 mW. The axial resolution is 9 μm and the mean beam spot size (in the focal plane) is 15 μm, making the RV approximately the size of one eukaryotic cell. The Thorlabs Swept source Optical Coherence Tomography Microscope software package (version 1.3.0.0, Thorlabs Inc.) was used for data acquisition.

2.2 Measuring Brownian motion from microsphere suspensions

To validate our data acquisition and analysis techniques we measured Brownian motion in monodisperse microsphere suspensions containing polystyrene microbeads (Polysciences, Warrington, PA) having mean diameters of 1.0 μm and 0.5 μm. The solutions were prepared at volume fractions of 0.5% and 1.27%, respectively. Both the distilled water used for the dilutions and the microsphere stock solutions were left at room temperature overnight to ensure consistency in temperature.

Data were acquired in the form of 14-bit OCT interference fringe signals. Two-dimensional frames containing 32 axial scans were recorded covering a transverse distance of 400 μm at a frame rate of 166Hz. A region of interest (ROI) measuring 32 pixels in the transverse direction and 8 pixels in the axial direction was selected starting at 30 μm below the sample surface (figure 1 (a)). For each pixel location, the signal intensity was plotted across all acquired frames (figure 1 (a) and (b)). A time fluctuation signal was obtained by subtracting the signal mean and dividing by the standard deviation. Since the autocorrelation (AC) function and the power spectrum of a signal are Fourier transform pairs [5], the autocorrelation of the time intensity signal at each pixel location was calculated by taking the inverse Fourier transform of its power spectrum.

The AC function from a suspension of monodisperse spherical particles undergoing Brownian motion decays exponentially and is described by the following equation for a homodyne system:

$$A(\tau) = e^{-2q^2 D_B t} \quad (1)$$

where the decorrelation time is $\tau = \frac{1}{2q^2 D_B}$. Here $q = \frac{4\pi}{\lambda}$ and D_B *is* the diffusion coefficient described by the Einstein-Stokes equation:

$$D_B = \frac{\kappa_B T}{6\pi\eta r} \quad (2)$$

where κ_B is Boltzmann's constant, T is the absolute temperature, η is the viscosity of the medium (in our case water) and r is the particle radius.

An exponential was fit to an average AC function obtained from the selected ROI and the DT was extracted using equation (1). Theoretical DTs for the two sizes of microspheres were calculated using equations (1) and (2).

2.3 Preparation of biological samples

Cell samples were prepared using centrifuged acute myeloid leukemia cells (AML-5, Ontario Cancer Institute, Toronto, Canada). Approximately 10^9 AML cells started from frozen stock samples were grown at 37° C in suspension flasks containing 150 mL of α-minimal essential medium supplemented with 1% streptomycin and 5% fetal bovine serum. Apoptosis was induced by treating cells with the chemotherapeutic agent cisplatin, a DNA intercalater, which causes a p53-dependent apoptosis in these cells [16]. Seven flasks were treated simultaneously at 10 μg/mL of cisplatin and returned to the incubator for up to 48 hours with one additional untreated flask to serve as a control. Each cell sample was prepared from a single flask. Imaging was carried out at 0, 2, 4, 6, 9, 12, 24 and 48 hours after cisplatin exposure. At each time, a cell sample was prepared for imaging from a single treated flask. Cells were washed with phosphate buffered saline and centrifuged in a bench top swing bucket centrifuge (Jouan CR4i, Thermo Fisher Scientific, Waltham, MA) in a flat bottom ependorff tube at 2000 *g* producing a densely packed cell pellet approximately 1 cm in diameter and 2 mm in thickness. The supernatant above the cell sample was carefully removed using a 200 μL pipette. Due to its short doubling time and its non-adherent nature, this cell line permits the rapid production of large numbers of cells for our measurements. Extensive use of AML cells in our laboratory for cell death monitoring using ultrasound techniques has permitted us to characterize the time kinetics of apoptosis in these cells [17-19]. The cell packing observed in the AML cell pellets resembles that seen in tumor xenografts *in vivo* and, thus, serves as a good model for cell death monitoring in tumors [20].

Multicellular tumor spheroids were prepared from HT-29 cells (ATCC: HTB-38), a colorectal adenocarcinoma cell line. Cells were maintained in McCoy's 5A modified medium (SIGMA) and supplemented with 5% fetal bovine serum and 1% streptomycin. Spheroids were grown by inoculating approximately 10^6 cells in 15mL of medium into a sterile 100mm Petri dish. After a period of 5 to 6 days cell aggregates were transferred to a new dish and medium was refreshed every 2 to 3 days. As they grew in size, the number of spheroids per dish was reduced to maintain a constant cell to growth medium ratio.

2.4 Data acquisition and analysis from biological samples

For AML cell pellets, data were acquired and autocorrelation functions computed for each pixel location in a similar manner to the microsphere suspensions described in section 2.1. A total of 10 sets of data were acquired from each AML sample. An average DT was calculated for each data set by measuring the half width of each AC function at half its maximum value.

Spheroid data were acquired with 128 axial scans spanning a transverse distance of 1mm. This larger field of view was used in order to capture the entire spheroid, but due to the increase in the number of axial scans the frame rate for this acquisition was reduced to 50 Hz. Autocorrelation functions were calculated for every pixel location in the spheroid images. In order to compare the DT between the core and the rim of the spheroids, a ROI in each region was selected

(figure 1(d)) and an average AC function was computed. To allow the spatial visualization of DTs within the different regions of the spheroid, a decorrelation map was generated by calculating the half-width at half maximum of the AC function at each pixel location and assigning grayscale values to the DTs.

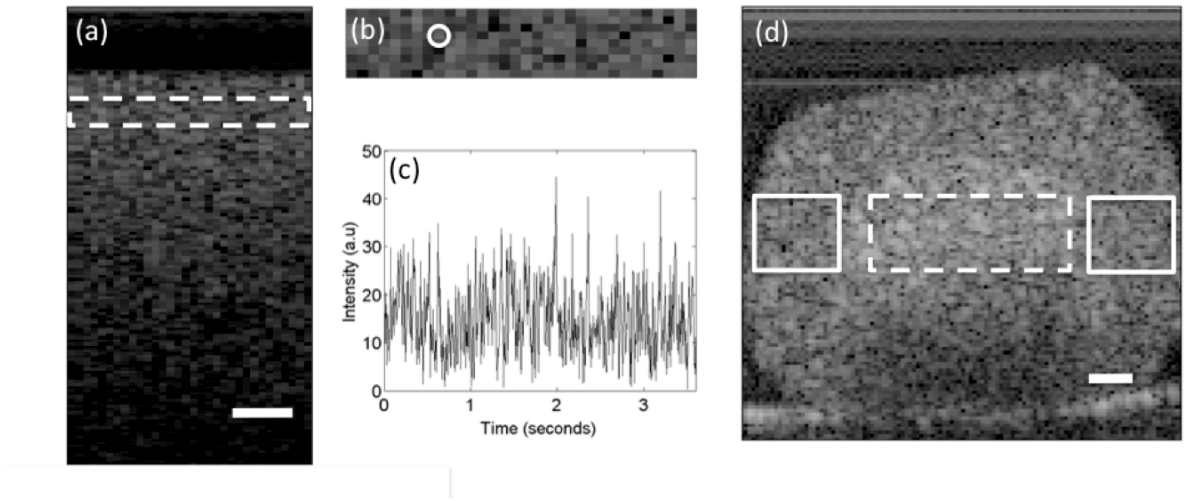

Figure 1. Analysis methods. (a) OCT b-mode image of a 1 μm polystyrene bead suspension. The ROI used for analysis is outlined by the dotted line. (b) The ROI outlined in (a) is enlarged and a single pixel outlined to illustrate the data analysis technique. (c) The intensity as a function of time for the pixel outlined in (b). (c) An OCT b-mode image of a spheroid. Regions from the spheroid edge (solid rectangles) and the spheroid core (dashed rectangle) were selected for analysis. The scale bars represent 100 μm.

2.5 Histological validation

Immediately after the completion of OCT imaging, cell pellets and spheroids were fixed in 10% formalin for 48 hours and subsequently paraffin embedded and processed for haematoxylin and eosin (H&E) staining. Microscopy was carried out using a Leica DM LB microscope and digital images were acquired with the Leica DC 200 digital imaging system (Leica Microsystems GmbH, Germany). Digital images obtained from H&E sections were used to observe cell and nuclear structure.

3. RESULTS AND DISCUSSION

3.1 Polystyrene bead suspensions

Autocorrelation functions obtained from microsphere suspensions are shown in figure 2 (a). As expected, the AC decays more rapidly for the smaller particles. The DT computed from exponential fits to these AC functions are plotted in figure 2 (b). These values are superimposed on a plot of the expected DT as a function of particle diameter obtained from equations (1) and (2). The experimental results are well matched to the theoretical curve, indicating that we are able to measure Brownian motion using OCT and validating our data acquisition and analysis techniques.

3.2 Apoptosis time course experiment

Histological sections stained with H&E (figure 3) obtained from AML cell samples indicated significant structural changes after 24 hours of cisplatin exposure. Nuclear condensation and fragmentation were observed as well as irregular cell shapes that may be indicative of cell membrane blebbing. Representative plots of the signal intensity fluctuations as a function of time from a single pixel are shown in figure 4. The backscatter fluctuations from the sample treated for 24 hours were higher in amplitude and more erratic, indicating more motion in the treated sample compared to the untreated control after 24 hours of cisplatin exposure. The average AC functions computed from the same two samples further confirmed this difference as the curve for the treated sample decayed more quickly. The DTs computed from cell samples obtained during two individual experiments are plotted as a function of treatment time in figure 5. Results from two separate experiments demonstrated good repeatability of this technique despite the biological variations that may have existed between the cells used in each experiment. This graph indicated a significant drop in DT after 24 and 48

hours of cisplatin exposure. The cell morphology observed in figure 3 suggests that these measurement times correspond to the stage in the apoptotic process where cell membrane blebbing and fragmentation may be occurring. We hypothesize that the significant drop in DT is related to an increase in intracellular motion caused by the cytoskeletal and membrane structural changes and reorganization required for this fragmentation.

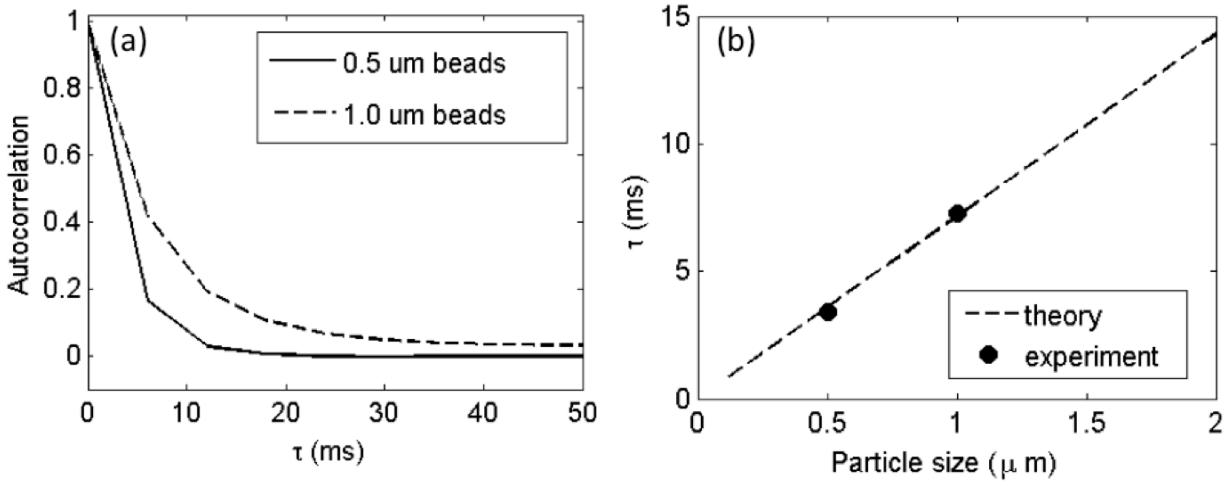

Figure 2. (a) Autocorrelation functions obtained from monodisperse microsphere suspensions. (b) Expected DT computed for monodisperse microsphere suspensions using the Einstein-Stokes equation. Experimental values of DT calculated from OCT data match the theoretical predictions.

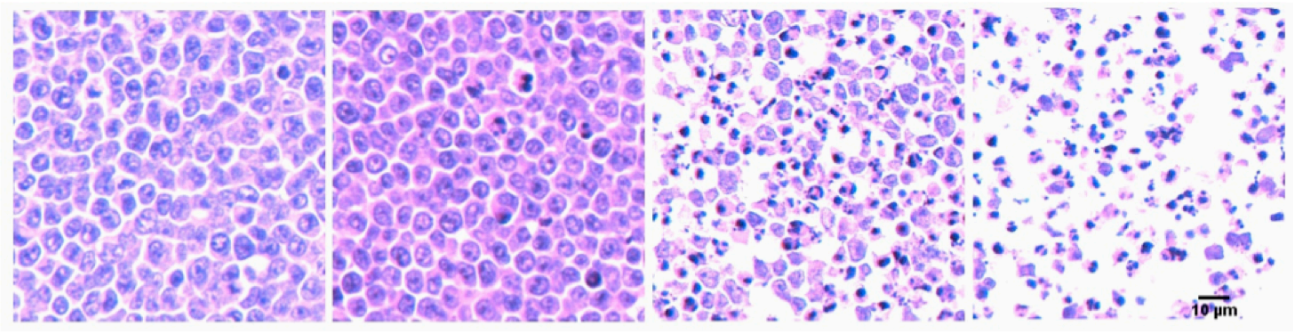

Figure 3. Representative H&E stained sections obtained from cisplatin treated cells after 0 hours (a), 12 hours (b), 24 hours (c) and 48 hours (d) of treatment.

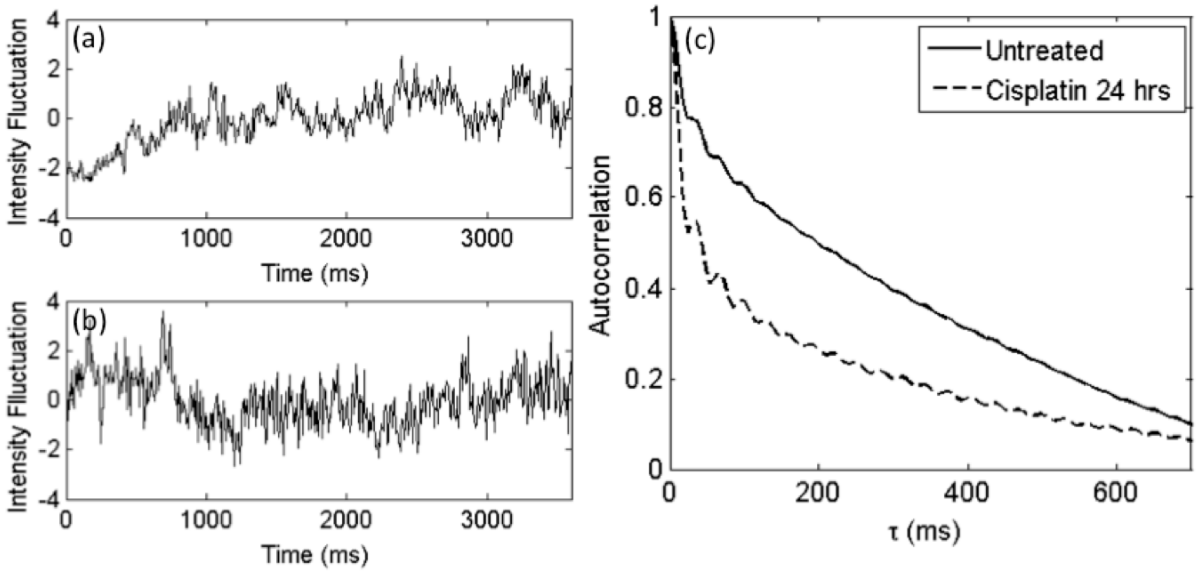

Figure 4. Data obtained from AML cell pellets. Intensity fluctuation as a function of time for a single pixel for (a) an untreated sample and (b) after 24 hours of cisplatin exposure. (c) Average autocorrelation functions computed from a selected ROI in AML cell pellets.

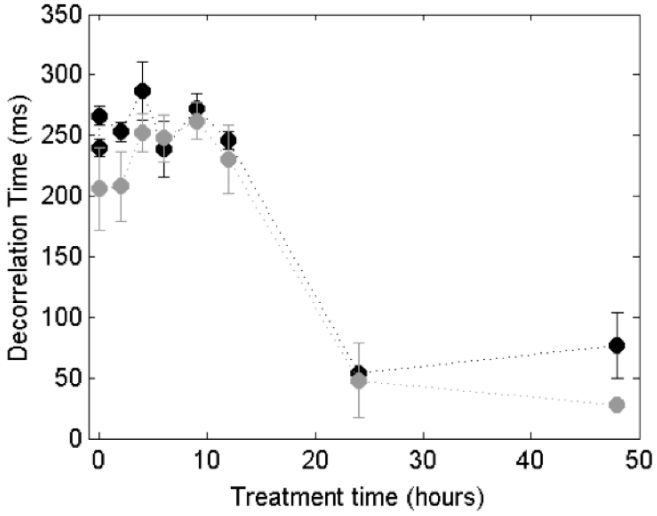

Figure 5. Decorrelation time computed from AML cell samples treated with cisplatin in two separate experiments. Error bars represent the standard deviation of 10 separate measurements from each sample.

3.3 Multicellular tumor spheroids

A histological section stained with H&E is shown in figure 6(a). The cells in the centre of the spheroid display nuclear condensation, as opposed to the viable cells observed at the edge of the spheroid, which present normal nuclear structure. The white areas in the centre of the spheroid are an artifact of histology and are indicative of cell death. Although the core of this spheroid does not yet display signs of necrosis, early signs of cell death (nuclear pyknosis) are present.

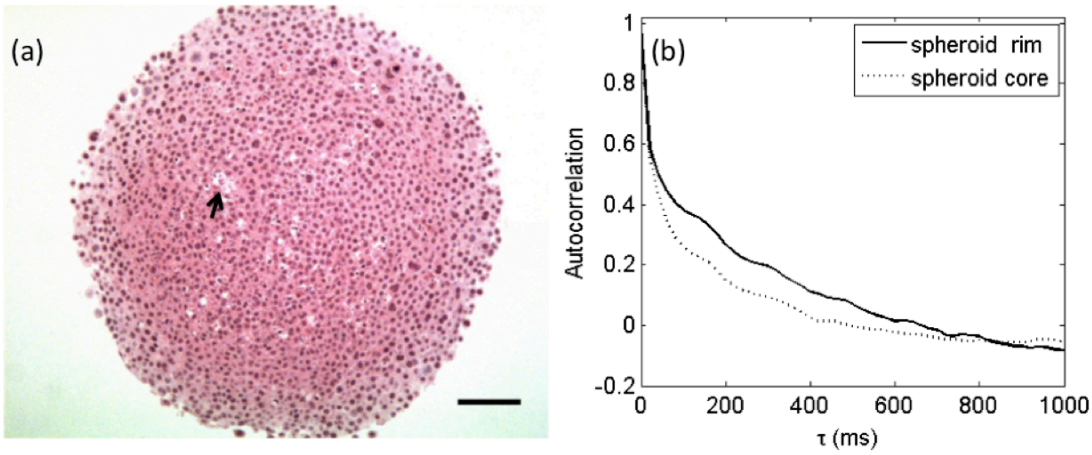

Figure 6. (a) H&E stained sections obtained from an HT-29 tumor spheroid. White regions (indicated by an arrow) are a sign of cell death. Scale bar represents 100 μm. (b) Autocorrelation functions calculated from the rim and the core regions of the tumor spheroid.

Autocorrelation functions computed from regions on the edge and in the core of the spheroid indicated a faster decay in the core region. We believe this is due to an increase in intracellular motion resulting from cell death as corroborated by the morphological differences between the core and edge of the spheroid observed in histology. The spatial differences in intracellular motion can be appreciated by examination of a map of DTs computed from the OCT data. In figure 7, an OCT backscatter image of the spheroid is shown on the left, indicating an increase in backscatter intensity in the core. We have previously related increases in backscatter intensity to cell death in AML cell samples [11]. In figure 7 (b), the DT for each pixel location of figure 7(a) is indicated by the grayscale bar shown to the right of the image, where darker values indicate shorter DT (or, equivalently, higher intracellular motion) and brighter values indicate longer DT, or less intracellular motion. In this figure, we observed a difference in DT between the centre and the edges of the spheroid, where shorter and longer DTs are indicated, respectively. This central region of increased intracellular motion also correlates with the region of increased backscatter intensity in figure 7 (a), further suggesting that a drop in DT is related to cell death. The black region at the bottom of figure 7 (b) is due to low signal to noise ratio in the OCT image and not a low DT.

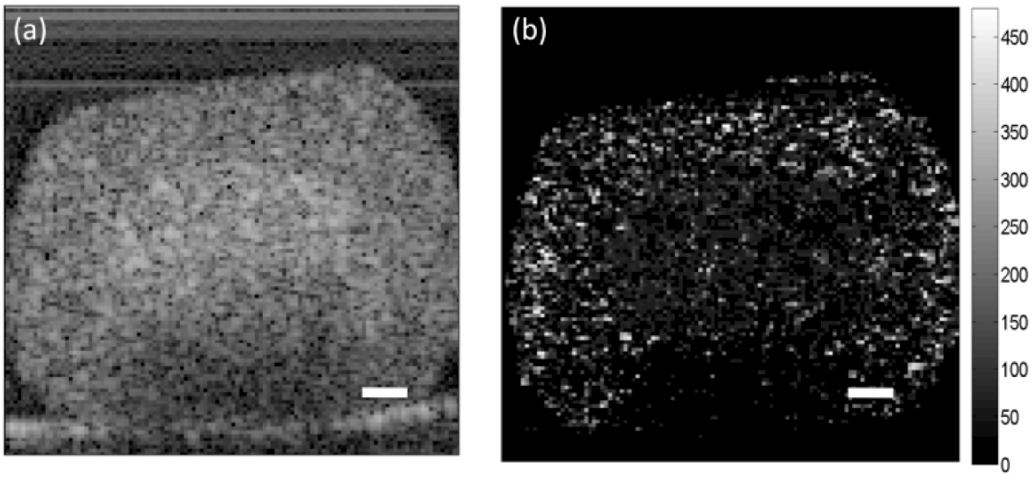

Figure 7. (a) OCT b-mode image of an HT-29 spheroid. Increased backscatter intensity is observed in the core of the spheroid. (b) Parametric image of DT for the spheroid depicted in (a). Shorter DTs in the core of the spheroid correspond with the regions of higher backscatter intensity. The scale bars represent 100 μm.

The resolution volume of our OCT system is approximately the size of a single cell. Scatterers giving rise to the signal intensity in each RV may include organelles, such as mitochondria and lysosomes, nuclear material, cytoskeletal components and the cell membrane. Any change in the spatial distribution and scattering strength of these scatterers can introduce fluctuations in the speckle intensity. Events that could modify the scatterer spatial distribution and scattering strength include movement or reorganization of the scatterers within the RV or the arrival and departure of scatterers into and out of this volume. A cell's contents are continuously moving due to various forces. Motion may be driven by active processes such as organelle transport by motor proteins along microtubules and actin filaments, or cytoskeletal restructuring during mitosis and apoptosis [21]. Diffusive transport of small organelles, vesicles and macromolecules is also present due to thermal processes (Brownian motion) as well as from the fluctuation of the cytoplasm caused by movement of motor-bound organelles and the cytoskeleton [22].

Assuming the dominant optical scatterers inside living cells are the mitochondria [23] and the nucleus [24], we expect to see a change in the rate of motion of cellular components during apoptosis due to mitochondrial and nuclear fragmentation. In addition to movement related to fragmentation, nuclear and mitochondrial fragments inside a cell will be subject to cytoplasmic motion caused by contractile forces of the cytoskeleton during membrane blebbing and the formation of apoptotic bodies. The period between the induction of apoptosis and the first morphological signs of cell death is asynchronous across a given population of cells and ranges between 2 to 48 hours. The duration of the execution phase (the period during which structural changes occur), however, is largely invariant and lasts approximately 2 to 4 hours [25]. Thus, the entire process of cell shrinkage, nuclear fragmentation, membrane blebbing and the formation of apoptotic bodies occurs over a relatively short time in a given apoptotic cell. It is, therefore, not surprising to see a significant drop in DT during apoptosis, indicating an increase in intracellular motion.

Several simple classical models exist for calculating the dynamic light scattering properties of systems of particles in motion [26]. These include models for the random (Brownian) motion of spherical particles suspended in a liquid medium, the uniform motion of particles subjected to an external force (flow) and the complicated movement of motile micro-organisms. The motion inside living cells is far more complex than any of the existing models, not only because of the various sources of intracellular motion, but also due to the large variation in size of subcellular components. A theoretical treatment of the dynamic light scattering properties of cells would likely include a combination of the above-mentioned models. We hypothesize that the shape of the AC function depends on the motion of the dominant scatterer in our sample, the cell type and the viability of the cell. Further investigation of the relationship of cell viability to the shape of the AC curve is the subject of future work.

We have demonstrated through an apoptosis time course experiment and spheroid imaging that our technique is repeatable and sensitive to variations in intracellular motion related to cell death. Since this dynamic light scattering technique relies on signal fluctuations rather than the absolute value of the signal intensity, the effects of signal attenuation and scattering angle are greatly reduced. For this reason we believe this method provides an advantage over techniques measuring backscatter strength for cell death detection. On the other hand, this method is more sensitive to the effects of bulk motion and blood flow *in vivo*. We are currently investigating methods to correct for motion artifacts in order to allow for *in vivo* implementation of this technique.

4. CONCLUSIONS

In summary, we have adapted concepts from dynamic light scattering and applied them to OCT to obtain measures of intracellular motion. Fluctuations in the OCT signal intensity caused by the Brownian motion of monodisperse microsphere suspensions were used to validate our technique. We have demonstrated in this study that this method can reliably detect changes in the rate of intracellular motion between viable and apoptotic cells *in vitro*. Application of this technique to the imaging of multicellular tumor spheroids confirmed the ability to generate a spatial map of the decorrelation times. It was found that areas with shorter DTs were spatially coincident with regions of increased OCT backscatter intensity. Based on previous work establishing that apoptosis causes an increase in backscatter intensity, these results further confirmed that a drop in decorrelation time is related to cell death. To our knowledge, this is the first time that dynamic light scattering has been applied to OCT for detecting apoptosis. Currently, feasibility studies are underway to investigate the implementation of this technique *in vivo* for detecting cell death in a mouse tumor model.

5. REFERENCES

[1] Schmitt, J., Xiang, S. and Yung, K., "Speckle in optical coherence tomography," Journal of Biomedical Optics, 4, 95 (1999).

[2] Jeong, K., Turek, J. and Nolte, D., "Volumetric motility-contrast imaging of tissue response to cytoskeletal anti-cancer drugs," Optics Express, 15(21), 14057-14064 (2007).

[3] Mariampillai, A., Standish, B. A., Moriyama, E. H., Khurana, M., Munce, N. R., Leung, M. K., Jiang, J., Cable, A., Wilson, B. C., Vitkin, I. A. and Yang, V. X., "Speckle variance detection of microvasculature using swept-source optical coherence tomography," Opt Lett, 33(13), 1530-2 (2008).

[4] Majno, G. and Joris, I., "Apoptosis, oncosis, and necrosis. An overview of cell death.," The American journal of pathology, 146(1), 3 (1995).

[5] Berne, B. and Pecora, R., [Dynamic Light Scattering] Dover Publications Inc., New York(1976).

[6] Miike, H., Hideshima, M., Hashimoto, H. and Ebina, Y., "Dynamic Laser-Light Scattering Study on Bacterial Growth," Japanese Journal of Applied Physics, 23(8), 1129-1132 (1984).

[7] Berge, P., Volochine, B., Billard, R. and Hamelin, A., "[Demonstration of the characteristic movement of living microorganisms owing to the study of the inelastic diffusion of light]," C R Acad Sci Hebd Seances Acad Sci D, 265(12), 889-92 (1967).

[8] Tanaka, T. and Benedek, G. B., "Measurement of the Velocity of Blood Flow (in vivo) Using a Fiber Optic Catheter and Optical Mixing Spectroscopy," Appl Opt, 14(1), 189-96 (1975).

[9] Boas, D. A. and Yodh, A. G., "Spatially varying dynamical properties of turbid media probed with diffusing temporal light correlation," Journal of the Optical Society of America A, 14(1), 192-215 (1997).

[10] Jeong, K., Turek, J. and Nolte, D., "Speckle fluctuation spectroscopy of intracellular motion in living tissue using coherence-domain digital holography," Journal of Biomedical Optics, 15, 030514 (2010).

[11] Farhat, G., Yang, V. X. D., Czarnota, G. and Kolios, M., "Detecting Cell Death with Optical Coherence Tomography and Envelope Statistics" (submitted).

[12] Strohm, E. M., Czarnota, G. J. and Kolios, M. C., "Quantitative measurements of apoptotic cell properties using acoustic microscopy," Ultrasonics, Ferroelectrics and Frequency Control, IEEE Transactions on, 57(10), 2293-2304 (2010).

[13] Czarnota, G., Kolios, M., Vaziri, H., Benchimol, S., Ottensmeyer, F., Sherar, M. and Hunt, J., "Ultrasonic biomicroscopy of viable, dead and apoptotic cells," Ultrasound in medicine & biology, 23(6), 961-965 (1997).

[14] Sutherland, R., Sordat, B., Bamat, J., Gabbert, H., Bourrat, B. and Mueller-Klieser, W., "Oxygenation and differentiation in multicellular spheroids of human colon carcinoma," Cancer Research, 46(10), 5320 (1986).

[15] Hauptmann, S., Gebauer-Hartung, P., Leclere, A., Denkert, C., Pest, S., Klosterhalfen, B. and Dietel, M., "Induction of apoptosis in the centre of multicellular tumour spheroids of colorectal adenocarcinomas—involvement of CD95 pathway and differentiation," Apoptosis, 3(4), 267-280 (1998).

[16] Zamble, D. and Lippard, S., "Cisplatin and DNA repair in cancer chemotherapy," Trends in biochemical sciences, 20(10), 435-439 (1995).

[17] Czarnota, G., Kolios, M., Abraham, J., Portnoy, M., Ottensmeyer, F., Hunt, J. and Sherar, M., "Ultrasound imaging of apoptosis: high-resolution non-invasive monitoring of programmed cell death in vitro, in situ and in vivo," British journal of cancer, 81(3), 520 (1999).

[18] Tunis, A., Czarnota, G., Giles, A., Sherar, M., Hunt, J. and Kolios, M., "Monitoring structural changes in cells with high-frequency ultrasound signal statistics," Ultrasound in medicine & biology, 31(8), 1041-1049 (2005).

[19] Kolios, M., Czarnota, G., Lee, M., Hunt, J. and Sherar, M., "Ultrasonic spectral parameter characterization of apoptosis," Ultrasound in medicine & biology, 28(5), 589-597 (2002).

[20] Vlad, R., [Quantitative ultrasound characterization of responses to radiotherapy in vitro and in vivo] University of Toronto, Toronto(2009).

[21] Kelleher, J. and Titus, M., "Intracellular motility: How can we all work together?," Current Biology, 8(11), R394-R397 (1998).

[22] Brangwynne, C. P., Koenderink, G. H., MacKintosh, F. C. and Weitz, D. A., "Cytoplasmic diffusion: molecular motors mix it up," The Journal of cell biology, 183(4), 583 (2008).

[23] Pasternack, R. Z., JY; Boustany, NN, "Optical scatter changes at the onset of apoptosis are spatially associated with mitochondria," Journal of Biomedical Optics, 15, 040504 (2010).

[24] Mourant, J., Canpolat, M., Brocker, C., Esponda-Ramos, O., Johnson, T., Matanock, A., Stetter, K. and Freyer, J., "Light scattering from cells: the contribution of the nucleus and the effects of proliferative status," Journal of Biomedical Optics, 5, 131 (2000).

[25] Mills, J. C., "Mechanisms underlying the hallmark features of the execution-phase of apoptosis," Advances in Cell Aging and Gerontology, 5, 1-38 (2001).
[26] Berne, B. and Pecora, R., "Laser Light Scattering from Liquids," Annual Review of Physical Chemistry, 25(1), 233-253 (1974).